Desalination and Water Treatment
www.deswater.com
doi: 10.5004/dwt.2022.28132

249 (2022) 61–73
February

Preparation of activated carbon from sludge by 'double green activation' and adsorption capacity for Congo red dye

Jun Chen[a,b,c,*], Xiaowan Dong[a,b], Sisi Cao[a,b], Layun Zhu[a,b], Zihui Song[a,b], Jie Jin[a,d], Hongxing Yang[b]

[a]*School of Biology, Food and Environment, Hefei University, Hefei 230601, China, Tel. +86 551 62158405; Fax: +86 551 62158406; emails: chenjun@hfuu.edu.cn (J. Chen), 1823641450@qq.com (X. Dong), 1241715398@qq.com (S. Cao), 2966705708@qq.com (L. Zhu), 2966705708@qq.com (Z. Song), Tel. +86 551 62158409; Fax: +86 551 62158406; email: 2378859912@qq.com (J. Jin)*
[b]*Anhui Key Laboratory of Sewage Purification and Eco-restoration Materials, Hefei 230088, China, Tel. +86 551 65326105; Fax: +86 551 62158406; email: 331279963@qq.com (H. Yang)*
[c]*Anhui Guoke Testing Technology Co., Ltd., Hefei 230041, China*

Received 21 August 2021; Accepted 3 January 2022

ABSTRACT

The sludge was transformed into activated carbon (SAC) by the green activation method. Citric acid ($C_6H_8O_7$) and potassium ferrate (K_2FeO_4) were used as different activators, and four kinds of SAC (SAC_N; SAC_{CA}; SAC_{PF}; $SAC_{CA\text{-}PF}$) were prepared by different activator combinations. The $SAC_{CA\text{-}PF}$ was produced with $C_6H_8O_7$ and K_2FeO_4 by the 'double green activation' method, it had the highest specific surface area (136 $m^2\ g^{-1}$) and abundant functional groups (C=O, Si–C) attached to it. The adsorption capacity of $SAC_{CA\text{-}PF}$ for Congo red (CR) was 98.61 mg g^{-1}, faster and more efficient than the other SAC. The adsorption process was well described by the Langmuir model and quasi-second-order kinetic model. The adsorption mechanism of $SAC_{CA\text{-}PF}$ (available on the CR surface) was attributed to various interactions, such as hydrogen bonding and electrostatic attraction. Moreover, $SAC_{CA\text{-}PF}$ could be regenerated by Fenton reaction, and the removal rate was still more than 80% after five cycles of used. The results indicated that the impregnation of $C_6H_8O_7$ and K_2FeO_4 can effectively improve the adsorption efficiency of SAC, prepared by the 'double green activation' method. This method can be applied for carbonized sludge and dye wastewater treatment in an environment-friendly way.

Keywords: SAC; Double green activation; Adsorption performance

1. Introduction

With the rapid increase in population, usage and the development of the sewage treatment industry have also increased. During the sewage treatment, a large number of surplus sludge is produced due to the separation and conversion of the wastewater. China produces about 65 million tons of sludge every year. Sludge contains a huge amount of organic matter, insoluble inorganic substances, etc. In this process, different types of microbe micelle form a variety of microbes. Hence, untreated sludge poses a great threat to human lives [1–3].

With the development of different materials, there have been many studies on biomass materials as raw materials of activated carbon to achieve the regeneration of resources [4]. The amount of harmful wastes has increased in the sludge. Hence, sludge treatment and disposal have become very important. Sludge has high water content and complex

* Corresponding author.

composition. It is a mixture of organic matters (maximum), inorganic matters, heavy metals, and microorganisms in the dissolved or suspended state, which is easy to decay. At present, the commonly used sludge disposal methods mainly include anaerobic digestion, incineration and landfill, compost making, land usage, and so on [5–7]. However, these methods are inefficient in separating different elements of the wastes; for example, sludge landfill, which is one of the disposal methods, may cause toxic leaching of heavy metals and occupy a large amount of land area, which may cause further environmental pollution [1,8].

Due to the difficulty of subsequent sludge disposal, it is a good idea to utilize the resources of sludge and make renewable materials, like sludge-based activated carbon (SAC) [9,10]. It not only solves the problem of environmental pollution caused by traditional sludge disposal but also reduces the high cost of raw materials used for producing activated carbon. Thus, the goal of 'killing two birds with one stone' can be achieved. At present, a large volume of research has been carried out research on the adsorption of dyes on activated carbon, such as powdered activated carbon, green activated carbon made of an orange tree wood, and tin sulfide nanoparticles loaded on activated carbon [11–15].

Several studies observed that the SAC could be used as a carbonized material, such as adsorbent, catalyst, lubricant, amendment, and electrode material, etc. The sludge-based adsorbents could be used to remove contaminants such as heavy metals, dyes, organic pollutants, phosphates, phenolic compounds, and other compounds from the environment [10,16–19]. However, the direct adsorption performance of SAC is poor due to its small specific surface area and pore volume, and large ash content. In recent years, many researchers have been trying to increase the performance of SAC, especially the specific surface area. For example, alkaline reagents and activators [20] can modify the activated sludge to produce derivative adsorbents. Some studies have shown that the mechanical strength of sludge can be improved by modifying the sludge with alkali and then using a cross-linking agent. Activation, which is divided into physical activation and chemical activation, is usually used to improve the specific surface area and adsorption capacity of the sludge carbon [21]. Physical and chemical techniques can be used to obtain activated carbon from bituminous coal and study the adsorption performance of textile dye basic blue 41 [22]. The specific surface area of the activated carbon prepared by modifying the organic waste with carbon dioxide is much larger than that of the water vapor-modified activated carbon [23]. Chemical activation refers to the addition of chemical agents for sludge impregnation and then adding inert gas as a protective gas for high-temperature carbonization. Compared with physical activation, it has the advantages of simple operation, low activation temperature, relatively short activation time, low energy consumption, and the generation of micropores and formation of many functional groups on the surface of the composite materials. However, it may corrode the equipment. At present, the chemical reagents used in the laboratory generally include KOH, NaOH, $ZnCl_2$, $FeCl_3$, H_2SO_4, H_3PO_4, uric acid and others. Yang et al. reported that $Fe_2(SO_4)_3$ efficiently activated the sludge-based carbon to adsorb tetracycline [24]. Used Fe_3O_4 modified sludge-based biochar was used to adsorb phosphate, and the effect was satisfactory. After impregnation with $FeCl_3$, the maximum adsorption capacity reached up to 111.0 mg g^{-1} [25]. Moreover, The adsorption mechanism of SAC on dissolved organic matter mainly includes pore filling, particle diffusion and distribution, hydrophilic and hydrophobic action, electrostatic action and hydrogen bonding, etc. [26].

In general, the chemical activation method can improve the specific surface area of the activated carbon, but the energy consumption is still relatively high in this process. In recent years, numerous studies have been reported on the usage of chemical activation at low temperatures (400°C–600°C). However, most of the activators are harmful to human health. For example, the strong alkali and the metallic zinc in zinc chloride (used in the activation process) must be treated to prevent secondary pollution. Therefore, future research should seek a new chemical agent.

In this paper, based on the resources of sludge, a chemical activation method is adopted, and environment-friendly activators such as citric acid ($C_6H_8O_7$) and K_2FeO_4 are selected to carry out the green carbonization of sludge. SAC with low cost and high efficiency was obtained. The effect of chemical substances on the modification of structural properties of SAC was studied, including microstructure, pore structure, elemental composition, and functional groups. The adsorption performance and mechanism of the prepared SAC for dye of Congo red (CR) were evaluated, and the application prospect of the SAC for dye of CR was also explored.

2. Materials and methods

2.1. Materials

The sludge used in the experiment was taken from the sewage treatment plant of the Hefei Economic Development Zone. K_2FeO_4, $C_6H_8O_7$, HCl (36.5%), NaOH, $FeSO_4{\cdot}7H_2O$, H_2O_2, CR, Methylene blue (MB), Rhodamine B (RB) were purchased from Sinopharm Chemical Reagent Co, Ltd. All chemicals were used without further purification, and the solutions were prepared by deionized water.

2.2. Preparation of SAC

To minimize impurity, the sludge was dried, crushed, and screened (80 mesh). The screened sludge samples were heated up to 500°C in the ceramic ark of a vertical tubular furnace at a rate of 5°C/min with a flow rate of 100 mL min^{-1}. The carbonization process was held for 2 h under the nitrogen ambiance. The samples were taken out after the furnace temperature dropped to 100°C and then kept in a dryer at room temperature. The obtained sample was soaked in 0.5 mol L^{-1} HCl for 2 h, filtered and washed with distilled water until it was neutral. Then the sludge carbon into powder was ground and passed through 200 mesh sieves. The SAC sample prepared without any activator was named SAC_N.

A certain mass of the sludge sample and a certain mass of $C_6H_8O_7$ or K_2FeO_4 solution was mixed at 40°C for 6 h (5 g sludge, 100 mL of 10 wt.% $C_6H_8O_7$ solutions; 5 g sludge, 100 mL 0.1 mol L^{-1} K_2FeO_4 mixed solutions; 5 g

sludge, 100 mL mixed solution containing 10 wt.% $C_6H_8O_7$ and 0.1 mol L^{-1} K_2FeO_4) and dried at 105°C to carbonize the obtained sample according to the carbonization method of SAC_N. The obtained sample was soaked and pickled with 0.5 mol L^{-1} HCl for 2 h, then filtered and washed with distilled water until neutral, then dried at 105°C and passed through 200 mesh sieve for retention spare. The SAC samples prepared with $C_6H_8O_7$, K_2FeO_4, and a mixture of $C_6H_8O_7$ and K_2FeO_4 were named SAC_{CA}, SAC_{PF}, and $SAC_{CA\text{-}PF}$, respectively.

2.3. Batch adsorption study

2.3.1. Determination of adsorption properties of SAC

Four kinds of SAC (0.2 g) (SAC_N, SAC_{CA}, SAC_{PF}, $SAC_{CA\text{-}PF}$) were added into 100 mL of CR solution with an initial concentration of 200 mg L^{-1}, respectively, and placed in a water bath with an oscillating chamber at 25°C at a speed of 100 rpm. During the oscillation process, samples were taken out after 4, 8, 16, 30, 60, 90, 120, 240, 480, 600, and 720 min and filtered using a filter membrane (0.45 μm). The absorbance was measured at 498 nm using a V5000 visible spectrophotometer, the results were mean values from duplicate experiments. The adsorption capacity and removal efficiency of different samples were calculated using Eqs. (1) and (2).

Adsorption capacity:

$$q = \frac{V\left(C_0 - C_t\right)}{m} \tag{1}$$

Removal efficiency:

$$R(\%) = \frac{\left(C_0 - C_t\right)}{C_0} \times 100 \tag{2}$$

where q (mg g^{-1}) is the adsorption capacity at the time, V (L) is the volume of adsorbent solution, C_0 (mg L^{-1}) is the initial mass concentration of adsorbent in solution, C_t is the mass concentration of adsorbent in the solution at the reaction time, m (g) is the mass of adsorbent, and R is the removal efficiency of the adsorbent solution.

2.3.2. Research methods of adsorption kinetics

The CR stock solution was diluted to 200 mg L^{-1}, and 100 mL aqueous dye solution was put into a conical flask (150 mL). The pH of the solution was considered as the initial pH. The prepared four kinds of SAC were added to the solution (0.2 g of SAC carbonized at 500°C, which was vibrated in a water bath oscillator at 25°C and 100 rpm). The solution was taken out at different intervals, like 4, 8, 16, 30, 60, 90, 120, 240, 480, 600, and 720 min, respectively, filtered with 0.45 μm of the filter membrane. The absorbance of each sample was measured at 498 nm, and the adsorption capacity was calculated.

2.3.3. Process to obtain adsorption isotherm

The CR stock solution was diluted to 100, 200, 300, 400 and 500 mg L^{-1}, respectively. Solution of 50 mL was put inside a 150 mL conical flask, 0.1 g of SAC was added into the flask, and then it was shaken at a constant temperature water bath oscillator at 25°C, 100 rpm for 12 h. After shaking, it was taken out, filtered with 0.45 μm of the filter membrane, and its absorbance was measured at 498 nm.

2.4. Analytical methods

The gold-plated samples were observed by scanning electron microscopy (SEM) using SU8010 cold-field emission scanning electron microscope (Hitachi Company, Japan). TD-3500 X-ray diffractometer (Dandong Tongda) was used to obtain X-ray diffraction (XRD) patterns of the samples. The X-ray photoelectron spectroscopic (XPS) spectra were obtained using the Thermo Fisher Kα XPS instrument (Thermo Field). The samples were scanned by the Nicolet IS 50+ Continuum Fourier-Transform Infrared Spectrometer (FTIR) (Thermo Fisher, USA). Raman spectra were obtained by the DXR laser confocal micro-Raman spectrometer (Thermo Fisher, USA). The pore size of the sample was determined by the nitrogen adsorption/desorption curves using a fully automated surface and porosity tester (Quantachrome, USA) and Brunauer–Emmett–Teller (BET) analysis. The zeta potential was measured by a particle size and zeta analyzer (Zetasizer Nano-ZS 90, Malvern, USA).

3. Results and discussion

3.1. Characterization of SAC adsorbent

Fine pores are seen on the surface of the pure SAC_N sample (Fig. 1a), while Fig. 1b and c show some rough flaked pores on the surface of the SAC_{CA}, SAC_{PF} samples (obtained by impregnation with $C_6H_8O_7$ and K_2FeO_4, respectively). The reason is that $C_6H_8O_7$ and K_2FeO_4 can cover the surface pores as well as react with the surface carbon to form rough pores. In Fig. 1d more circular apertures appear on the surface. It was mainly due to the fact that these two materials can decompose through the coupling action at high temperatures and generate gas, which may form mesopores on the surface. This also confirmed the successful synthesis of SAC.

XRD peaks of the samples are shown in Fig. 2a. The reflections at 2θ = 26.603°, 43.450°, 46.333°, 54.793°, 56.667° corresponded to quartz (JCPDS Card NO: 26-1079). The results indicated that the $SAC_{CA\text{-}PF}$ was graphitized. Three major peaks with the binding energy of 284.2 (±0.3 eV), 285.1 (±0.3 eV), and 288.7 (±0.3 eV) can be identified as C–C (C=C), C–O, and O–C=O, which were obtained by dividing the C1s spectra. The result was consistent with the literature data [27].

The FTIR spectra of SAC (Fig. 3a) indicate the presence of a large number of carbon and oxygen-containing functional groups in the material. The peak value around 777 cm^{-1} was considered to be the stretching vibration mode of Si–C. The peak value of 827 cm^{-1} was the symmetric stretching peak of Si–O–Si. The peak at 1,000 cm^{-1} was the C–O peak of the P–O–C anti-symmetric stretching vibration. The peak values at 1,500 and 1,588 cm^{-1} were the C=C stretching vibration peaks. In the infrared spectrum of SAC, in addition to the above peaks, there were also some characteristic absorption peaks. The peak of 2,000 cm^{-1} was the stretching vibration peak of metal carbonyl (C=O).

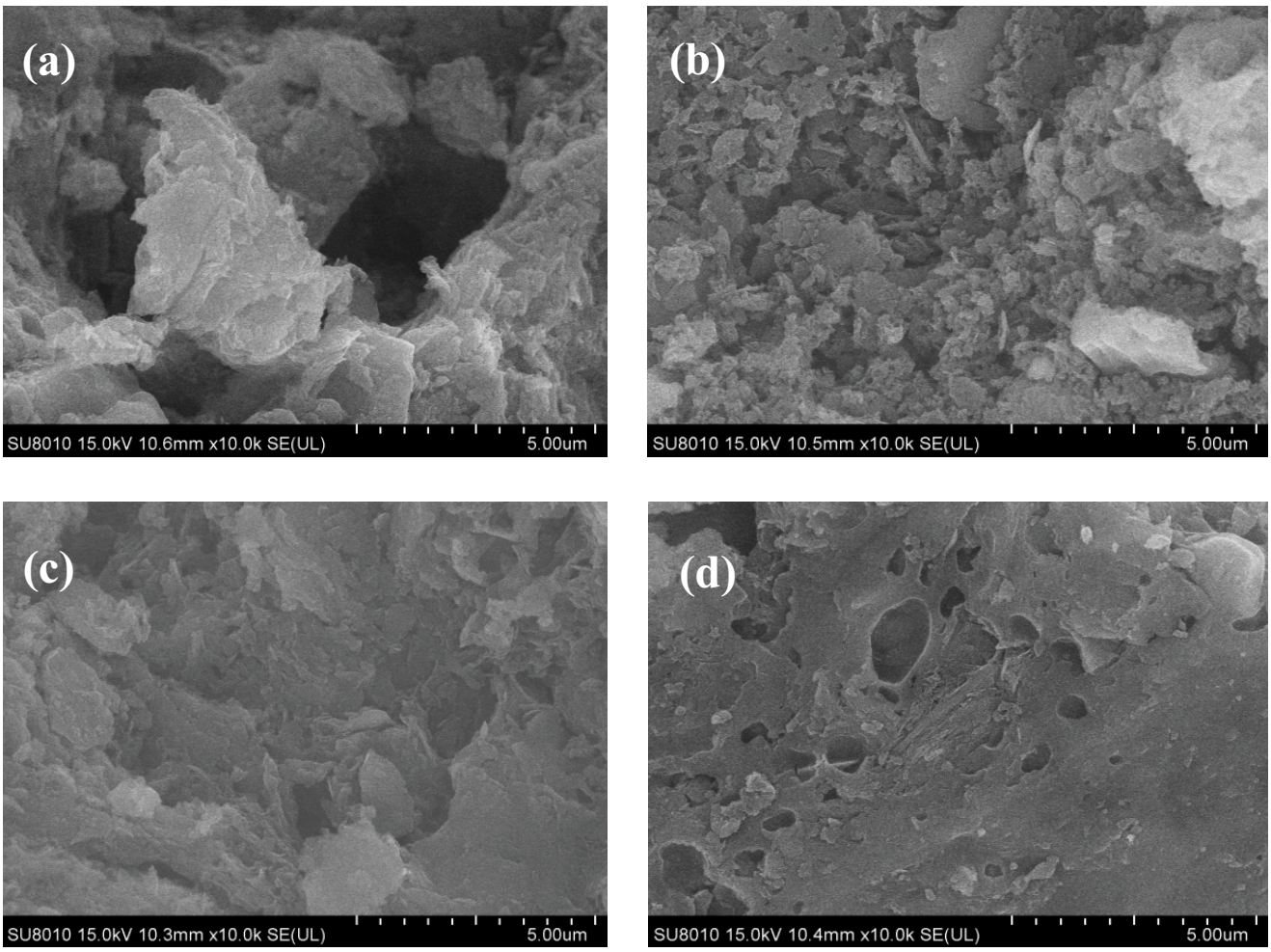

Fig. 1. SEM images of (a) SAC_N, (b) SAC_{CA}, (c) SAC_{PF}, and (d) $SAC_{CA\text{-}PF}$.

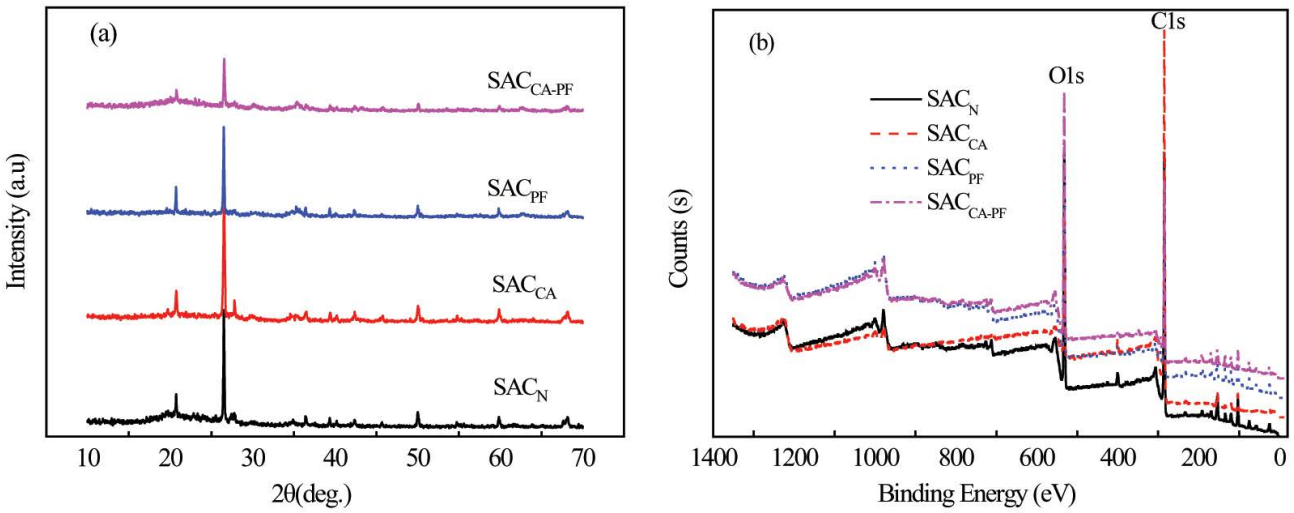

Fig. 2. (a) XRD and (b) XPS patterns of SAC_N, SAC_{CA}, SAC_{PF} and $SAC_{CA\text{-}PF}$.

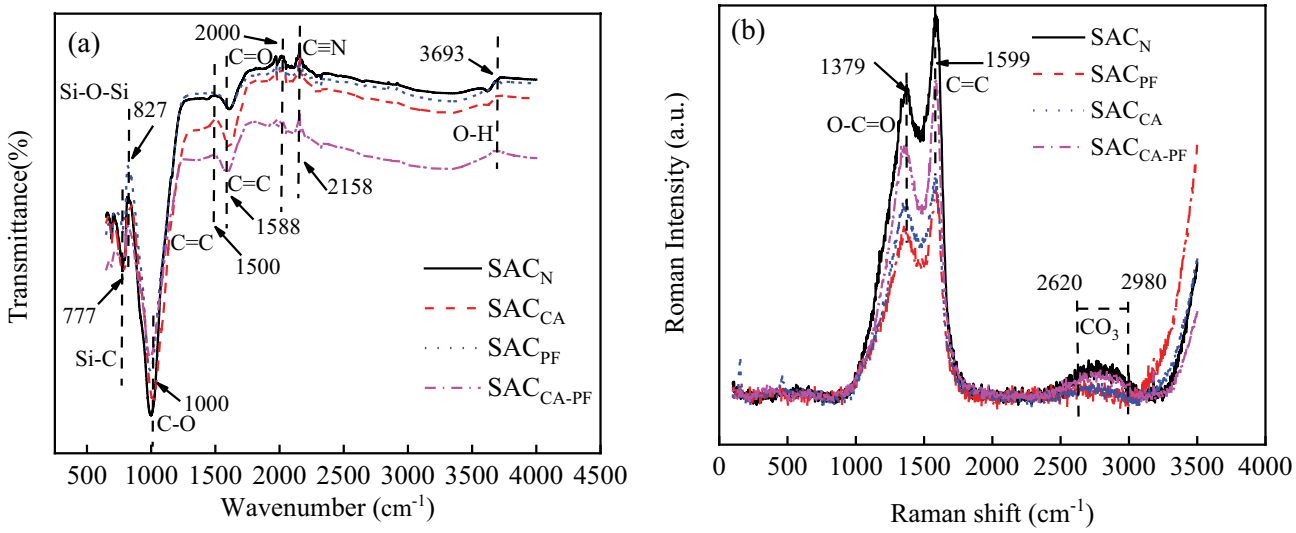

Fig. 3. (a) FTIR spectra and (b) Raman spectra of SAC_N, SAC_{CA}, SAC_{PF} and $SAC_{CA\text{-}PF}$.

The peak at 2,158 cm^{-1} was the vibration peak of C≡N of the metal thiocyanate salt M–S–C≡N. The 3,693 cm^{-1} peak corresponded to the O–H stretching vibration band of $C_6H_8O_7$. The existence of this hydrophilic functional group enhanced the hydrophilicity of the SAC, which was conducive to the removal of dyes. The results showed that $SAC_{CA\text{-}PF}$ was successfully prepared by the coupling reaction of $C_6H_8O_7$ and K_2FeO_4 [28,29].

The symmetric stretching motion of O–C=O of carboxylate occurs at the peak value of 1,379 cm^{-1}, which was related to the type and coordination mode of metal ions, as shown in Fig. 3b. Therefore, it can be concluded that Fe ions and carboxylate form a monodentate coordination compound. The peak at 1,599 cm^{-1} corresponds to the stretching vibration of C=C (Fig. 3a). At 2,620 and 2,980 cm^{-1}, the first frequency doubling peaks appeared which resonate with the anti-symmetric stretching vibration peaks of CO_3. This confirmed that $C_6H_8O_7$ and K_2FeO_4 cover the surface of SAC [30].

Fig. 4 shows the BET and Barrett–Joyner–Halenda (BJH) results of $SAC_{CA\text{-}PF}$. The presence of unclosed hysteresis loops and mesoporous structures was observed in the samples, which was mainly attributed to the instability of component condensation in the pores. Fig. 4a shows that $SAC_{CA\text{-}PF}$ sample had the strongest hysteresis loop effect, and the hysteresis loop was the H_4 type, which was a slit pore that often appears on the activated carbon adsorbent mixed with micropores and mesopores. Similarly, the type-I isotherm characteristics also indicated micropores which proved that $SAC_{CA\text{-}PF}$ had a strong adsorption capacity [31]. This result was consistent with the BJH pore size distribution. As shown in Fig. 4b, the pore size distribution peaks of the samples are all between 0 and 5 nm, indicating that $SAC_{CA\text{-}PF}$ forms micropores and small mesopores [29,32].

Table 1 compares and analyzes the specific surface area parameters of the four types of SAC. It was found that the specific surface area of the directly carbonized SAC was about 35.698 $m^2\ g^{-1}$, and the total pore volume was

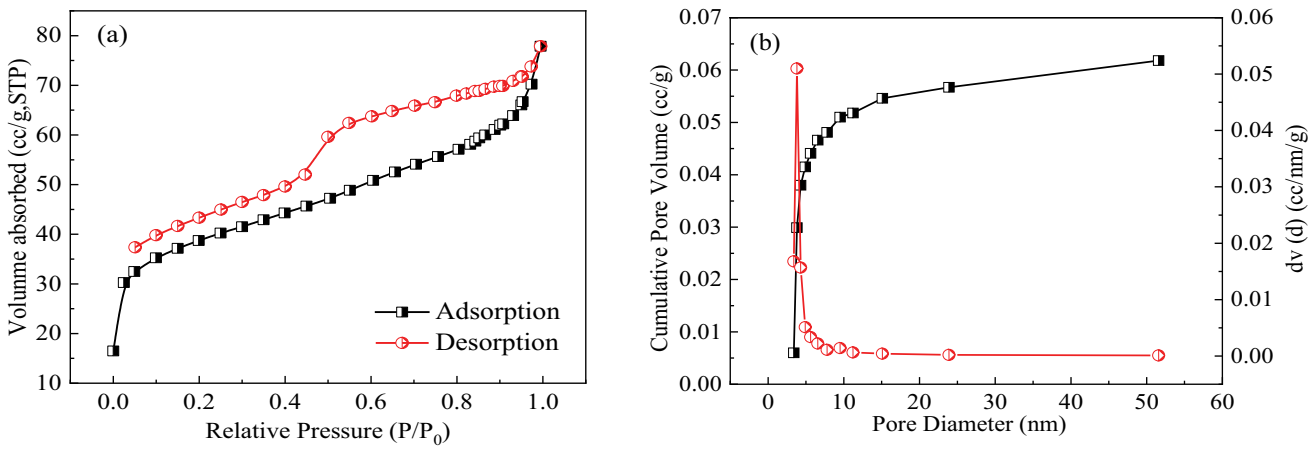

Fig. 4. (a) N_2 adsorption–desorption isotherm and (b) BJH desorption pore size distribution of $SAC_{CA\text{-}PF}$.

Table 1
BET and BJH analysis of SAC

Adsorbents	Average pore diameter (nm)	Total pore volume ($cm^3\ g^{-1}$)	Specific surface area ($m^2\ g^{-1}$)
SAC_N	9.9501	0.1259	35.698
SAC_{CA}	48.0248	0.1163	37.585
SAC_{PF}	45.3295	0.1569	69.571
$SAC_{CA\text{-}PF}$	12.3092	0.1205	136.339

0.1259 $cm^3\ g^{-1}$. The specific surface area increased slightly because the surface was covered by $C_6H_8O_7$ and K_2FeO_4. The specific surface area of $SAC_{CA\text{-}PF}$ was greatly increased up to 136.339 $m^2\ g^{-1}$, which was larger than that of SAC_N, SAC_{CA} and SAC_{PF}. The pore size and total pore volume were 12.3092 nm and 0.1205 $cm^3\ g^{-1}$ [33].

3.2. Effect of different adsorbents by SAC

The adsorption capacity of different SAC was displayed in Fig. 5.

From the adsorption performance of the four types of SAC (Fig. 5), it was found that the adsorption effect of $SAC_{CA\text{-}PF}$ was significantly higher than that of the other three SAC, and it could reach the adsorption equilibrium in about 120 min, with the adsorption capacity up to 98.61 mg g^{-1}, 1.6 times than the SAC_N. The results indicated that the specific surface area and pore volume of SAC can be significantly increased by the coupling reaction of K_2FeO_4 and $C_6H_8O_7$. K_2FeO_4 was a strong oxidant, and $C_6H_8O_7$ can decompose and generate carbon dioxide gas at high temperatures and can also generate a certain pore structure on the surface of the SAC [34].

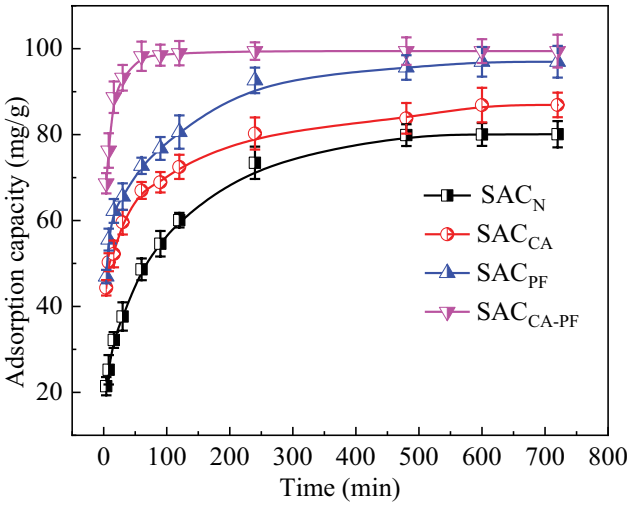

Fig. 5. Comparison of adsorption capacity of four different SAC (CR: 200 mg L^{-1}; *T*: 25°C; pH: 6; dose of SAC: 0.2 g).

3.3. Effect of pH and temperature on adsorbents of SAC

The effects of pH and temperature on adsorption efficiency were evaluated, and the results are shown in Fig. 6a and b. In order to investigate the influence of the initial pH value of the solution on the adsorption performance of ionic dyes, it was very important to measure the zeta potential of adsorbent and get the point of zero charge (pH_{pzc}) value of adsorbent. The pH_{pzc} values of the four SAC are shown in Fig. 6a (insert).

It can be seen that the zeta potential values of the four adsorbents were positive when pH was 2, and negative when pH was 4–10. The pH_{pzc} values of the four materials were all low (2.0–4.0), which was due to the fact that CA and K_2FeO_4 contain acidic groups on their surfaces to provide negative charge, thus attracting more H^+ and generating positive potential. Therefore, the zeta values of the four SAC were positive at lower pH [35]. Meanwhile, $SAC_{CA\text{-}PF}$ had the best adsorption effect, with adsorption capacity up to 99.63 mg g^{-1}. In addition, at any pH, the CR removal rate of $SAC_{CA\text{-}PF}$ was higher than that of the other three SAC, indicated that the CR removal rate of $SAC_{CA\text{-}PF}$ was significantly improved due to the coupling effect of the two reagents. With the increased of pH, the adsorption capacity of SAC decreased gradually, indicated that the adsorption performance of SAC was better in low pH environment. Due to the low pH value, the carboxyl and hydroxyl groups on the surface of SAC were positively charged. After protonation of CR, the anionic dye sulfonate group was decomposed into sulfonate anions, which increased electrostatic attraction and corresponded to the increase of zeta potential [36]. On the contrary, when the pH value was high, the adsorbent had a negative charge and generated electrostatic repulsion with the anionic dye, thus reducing the adsorption capacity. This was consistent with the analysis of potential value [30]. This phenomenon had also been explained in other studies, suggesting that the surface charge distribution and properties of SAC were affected by strong acids and bases. Thus, the electrostatic interaction between SAC and CR dye was changed [37]. The initial pH of the solution was 6. It can be seen that when the pH was lower than 6, there was little difference in the adsorption performance of different types of SAC. When pH was 6, the effect of SAC was better than that of pH 4, and the effect gradually decreased [38]. For finding the influence of temperature on the adsorption of dye by SAC, three temperature gradients were selected in this study. It can be clearly seen that the lower temperature was not conducive to the adsorption, which may be due to the fact that at the lower temperature, the kinetic energy of CR molecules was less, which results in less contact between the SAC and CR molecule. However, when the temperature increased, the degree of activation of ions in the solution also increased

[39]. However, when the temperature reached a certain level, the adsorption capacity attained a steady state.

3.4. Adsorption kinetics

For understanding the adsorption and diffusion process of SAC, the kinetic data were fitted to the pseudo-first-order and pseudo-second-order kinetic models and intraparticle diffusion models. Lagergren equation [Eq. (3)], pseudo-second-order equation [Eq. (4)] and Weber-Morris intraparticle diffusion equation [Eq. (5)] are respectively expressed as [40]:

$$\log(q_e - q_t) = \log q_e - k_1 t \tag{3}$$

$$\frac{t}{q} = \frac{1}{k_2 \cdot q_e^{\,2}} + \frac{1}{q_e} t \tag{4}$$

$$q_t = k \cdot t^{0.5} + b \tag{5}$$

where q_e (mg g^{-1}) is the adsorption capacity at equilibrium time, q_t (mg g^{-1}) is the adsorption capacity at t time; k_1 (min^{-1}) and k_2 (g mg^{-1} min^{-1}) are the first-order and second-order adsorption rate constants, respectively, and t (min) is the time. k (mg g^{-1} min$^{-0.5}$) is the internal diffusion rate constant, and intercept b reflects the boundary layer effect. The results are shown in Figs. 7 & 8 and Table 2.

By comparing Fig. 7a and b, it can be seen that the simulation effect of the second-order adsorption kinetic model on the CR adsorption behavior of the four kinds of

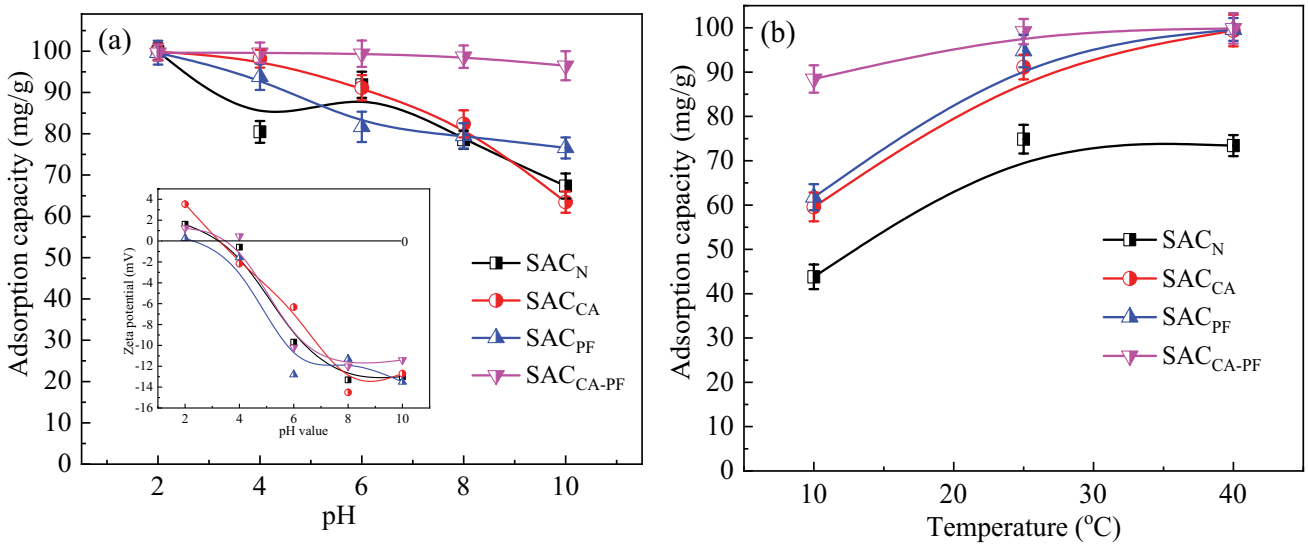

Fig. 6. The effects of (a) pH (inset: zeta potential of SAC at different pH) and (b) temperature on the adsorption of CR by four different SAC (CR: 200 mg L^{-1}; dose of SAC: 0.2 g; time: 720 min).

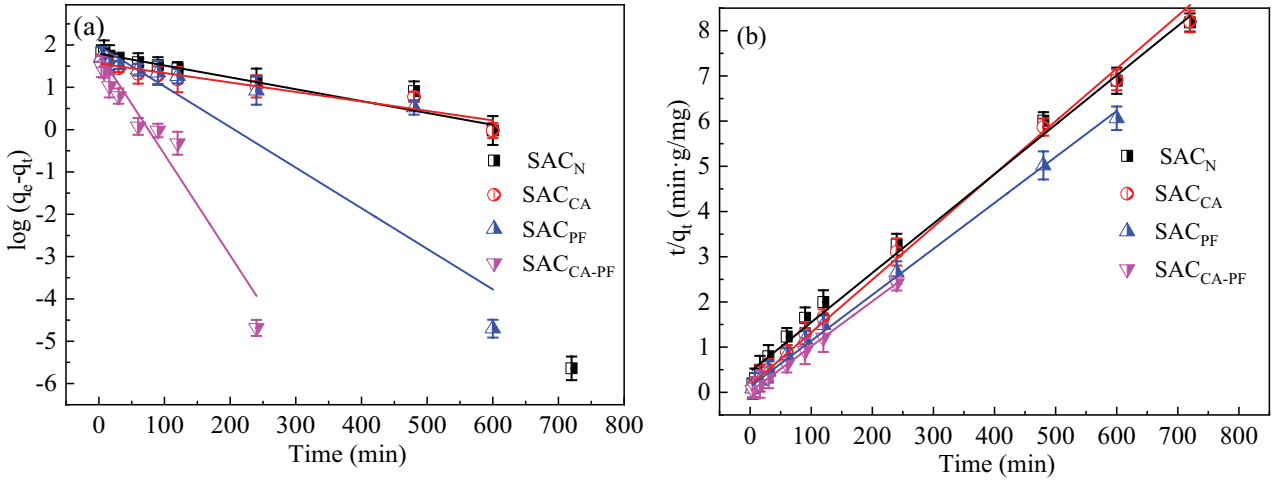

Fig. 7. (a) Pseudo-first-order kinetic model and (b) pseudo-second-order kinetic model of CR adsorption by four SAC (CR: 200 mg L^{-1}; T: 25°C; pH: 6; dose of SAC: 0.2 g; time: 720 min).

SAC was more consistent than that of the first-order kinetic model. Similar kinetic model results were observed for the different adsorbent-dye systems in the literature [41,42]. However, the two kinetic models showed a higher efficiency in simulating the adsorption behavior of SAC_{CA-PF} than the other three kinds of SAC. In Table 2 all the values of correlation coefficient R^2, obtained after second-order dynamic simulation, were greater than 0.99, and the correlation coefficient R^2 of SAC_{CA-PF} reached up to 0.99. Besides, the calculated value of equilibrium adsorption (q_e) of SAC_N, simulated by the second-order kinetics, was about 91.075, which was significantly different from the experimental value (87.99). The other three calculated values of equilibrium adsorption look almost the same as that of the experimental values (including the experimental errors). Therefore, according to the above analysis, the values of CR dye adsorption behavior of SAC simulated by the second-order kinetic model look more consistent. The observed results look more consistent with the chemical adsorption phenomenon, and electrostatic attraction might be the main driving force for the adsorption [43]. Comparison of the R^2 values obtained from the first-order kinetic model and the intraparticle diffusion model (Table 2 and Fig. 7) shows that physical adsorption and intraparticle diffusion contribute to the adsorption of CR by SAC [6]. The whole adsorption process can be classified into two parts. The intercept of the former stage is lower than that of the second stage, so the former stage was mainly affected by intraparticle diffusion and membrane diffusion. From the perspective of K_{P1}, the diffusion constant of SAC_N was the smallest while the value that of SAC_{CA-PF} was the largest. In addition, the line shown in Fig. 8 does not pass through the origin, which indicates the existence of boundary layer adsorption, which was consistent with the previous dynamic simulation.

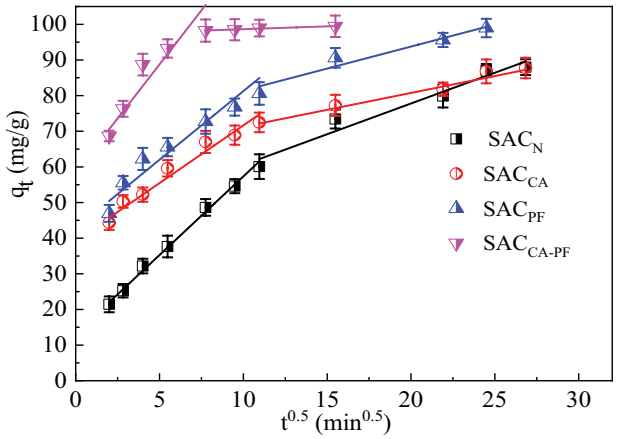

Fig. 8. Intraparticle diffusion model of CR adsorption by four SAC (CR: 200 mg L^{-1}; T: 25°C; pH: 6; dose of SAC: 0.2 g; time: 720 min).

3.5. Adsorption isotherms

Adsorption isotherm refers to the relationship between the adsorbate in the liquid phase and the adsorbate adsorbed on the surface of the adsorbent at equilibrium at a certain temperature. By fitting the adsorption isotherm with the adsorption model, the maximum adsorption capacity of the adsorbents can be calculated. Commonly used adsorption isotherm fitting models include Langmuir and Freundlich adsorption models. Freundlich isotherm model was often used to describe the multilayer adsorption of the adsorption solution by the adsorbents [44]. Langmuir isothermal model [Eq. (6)] and Freundlich isothermal model [Eq. (7)] are expressed below:

$$\frac{1}{q_e} = \frac{1}{Q_m} + \frac{1}{Q_m K_L}\frac{1}{C_e} \tag{6}$$

$$\log q_e = \log K_f + \frac{1}{n}\log C_e \tag{7}$$

where q_e (mg g^{-1}) is the amount of adsorption at the equilibrium of the adsorbent, Q_m (mg g^{-1}) is the Langmuir saturated amount of adsorption, C_e is the equilibrium concentration of adsorbate in solution (mg L^{-1}), K_L is the Langmuir adsorption constant, Q_m reflects the adsorption capacity of adsorbates by the adsorbents. The higher the Q_m value, the stronger

Table 2
The kinetic parameters and intraparticle diffusion parameters of SAC

Adsorbents	First-order kinetic model			Second-order kinetic model			Intraparticle diffusion parameters	
	q_e (mg g^{-1})	k_1 (min^{-1})	R^2	q_e (mg g^{-1})	k_2 (g mg^{-1} min^{-1})	R^2	K_{P1} K_{P2} (mg (g $min^{1/2})^{-1}$)	R_1^2 R_2^2
SAC_N	149	0.015	0.646	91.075	0.00026	0.995	4.331 1.709	0.996 0.958
SAC_{CA}	35.313	0.005	0.920	88.106	0.00067	0.998	3.065 0.971	0.967 0.980
SAC_{PF}	96.022	0.018	0.698	99.900	0.00060	0.998	3.410 1.270	0.950 0.948
SAC_{CA-PF}	49.041	0.056	0.946	100.402	0.00502	0.999	5.041 0.156	0.880 0.952

is the adsorption capacity. K_L reflects the binding ability of the adsorbent to the adsorbent site. $1/n$ is the constant related to the maximum adsorption capacity and adsorption energy, K_f is the Freundlich adsorption constant.

Fig. 9a and b shown the Langmuir adsorption isotherm and the Freundlich adsorption isotherm, respectively. The simulation efficiency of the Langmuir adsorption isotherm looked better than that of the Freundlich isotherm, and its correlation coefficients R^2 were all greater than that of the Freundlich isotherm, which showed that the adsorption process was mainly of monolithic nature. The obtained isotherm results were in agreement with the previous studies [45–47].

However, all n values (Table 3) obtained from the Freundlich isotherm were greater than 1, which proves that it is favorable for adsorption. Besides SAC_N, all the correlation coefficient values (R^2) of the other three types of SAC are greater than 0.99. Therefore, the adsorption of CR by SAC conformed to the Langmuir thermodynamic model, where the adsorption heat was independent of the surface coverage rate [38].

3.6. Adsorption mechanism

In this study, the used activators $C_6H_8O_7$ and K_2FeO_4 both formed pores. Compared with the sludge charcoal, which was directly carbonized, the specific surface area of SAC samples prepared using the activators was improved. In the process of $C_6H_8O_7$ pyrolysis, carbon dioxide was evolved, and large pores were generated during the process of sludge carbonization. However, when K_2FeO_4 was heated, it decomposed and produced oxygen under the acidic condition, forming mesopores and micropores. The SAC prepared by coupling the $C_6H_8O_7$ and K_2FeO_4 had a special pore structure, and mesopores and micropores were generated in the macropores. The $C_6H_8O_7$ and K_2FeO_4 used in the study are both green chemical agents and the double coupling effect of the two changes the characteristics of the SAC. In addition, neither of them causes secondary pollution. It had opened up the field of sludge resource utilization, implemented effective treatment and disposal of residual sludge, and also realized the purpose of treating waste by waste, and achieved remarkable results. The Fig. 10 showed the chemical structure of the SAC adsorbent and its binding mechanism with the CR dye, which can be attributed to various types of interactions. K_2FeO_4 can be reduced to ferric iron at high temperatures under acidic conditions, so iron-rich adsorbents can electrostatically bind the anionic reactive dyes. Some adsorbents that adsorb dye molecules of opposite charges through the charged groups present on the surface, such as sludge adsorbents modified by KOH, had hydroxyl groups on the surface, hydrogen bonds between the nitrogen atoms in the dye molecules, and electrostatic attraction and van der Waals forces to bind the reactive dyes containing amino groups [30,36,48]. Therefore, the SAC produced in this study can be used to electrostatically bind the reactive anionic dyes.

$$C_6H_8O_7 \cdot H_2O \rightarrow C_5H_6O_5 + H_2O + CO_2 \uparrow \quad (8)$$

$$4K_2FeO_4 \rightarrow 2Fe_2O_3 + 3O_2 \uparrow + 4K_2O \quad (9)$$

$$4FeO_4^{2-} + 20H^+ \rightarrow 10H_2O + 4Fe^{3+} + 3O_2 \uparrow \quad (10)$$

3.7. Color retention of adsorbent and adsorbent regeneration

3.7.1. Color retention capacity of the SAC

The SAC samples were removed from the non-woven fabric and cleaned until no more dye was coming out of it. Then, the weights of the samples were recorded, and the weights were measured again after the samples were centrifuged (at 1,000; 2,000; 3,000 rpm) for 10 min. The color retention capacity of the SAC was calculated by the change in the CR solution and adsorbent mass.

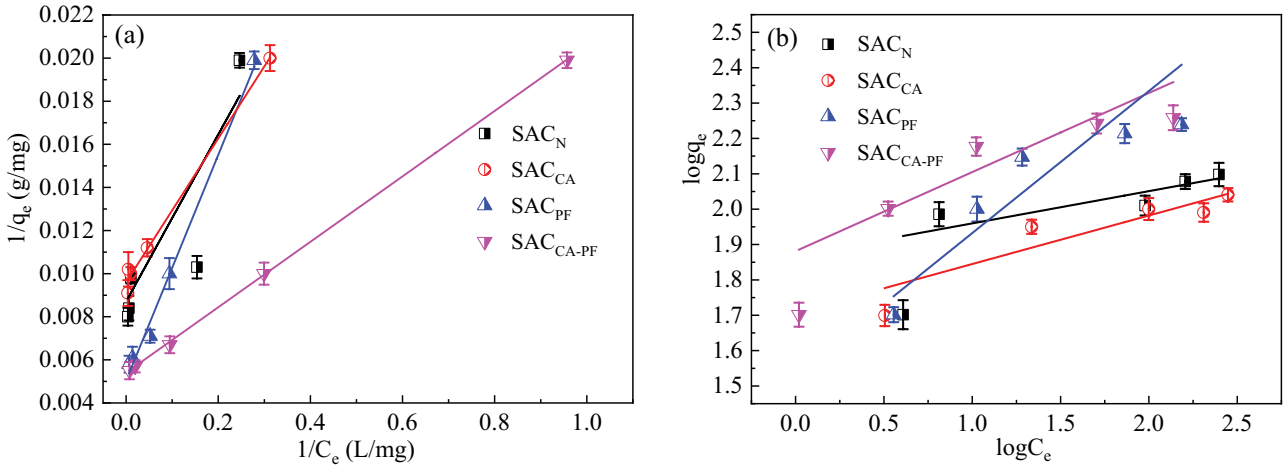

Fig. 9. (a) Langmuir isotherm model and (b) Freundlich isotherm model of CR adsorption by four SAC (T: 25°C; pH: 6; dose of SAC: 0.2 g; time: 720 min).

Table 3
Freundlich and Langmuir adsorption isotherm simulation parameters

Adsorbents	Langmuir			Freundlich		
	Q_m (mg g^{-1})	K_L (L mg^{-1})	R^2	n	K_f (mg/g (mg/L)$^{-1/n}$)	R^2
SAC_N	125.313	0.203	0.710	6.298	5.588	0.574
SAC_{CA}	104.384	0.287	0.990	6.314	5.280	0.828
SAC_{PF}	196.464	0.096	0.992	3.219	5.109	0.783
$SAC_{CA\text{-}PF}$	186.220	0.353	0.999	4.037	6.100	0.778

$$\text{Color retention capacity}(\%) = \frac{W_t'}{W_t} \quad (11)$$

where W_t' is the weight of each SAC sample after centrifuging for 10 min.

As shown in Fig. 11, the color retention capacity of $SAC_{CA\text{-}PF}$ dose not decreased with the increased in eccentricity after the adsorption of dyes. Possibly, $SAC_{CA\text{-}PF}$ closely binds with the functional groups present in CR rather than adsorbing. This result demonstrated that the adsorption data could be well simulated using the quasi-second-order adsorption kinetics model (Fig. 7 and Table 2). These results suggested that $SAC_{CA\text{-}PF}$ had a good retention performance and has a broad prospect in practical application.

3.7.2. Adsorbent regeneration of SAC

The Fenton oxidation method was used to regenerate the $SAC_{CA\text{-}PF}$ after it had been used to adsorb the dyes (the Fenton's reagent was composed of $FeSO_4{\cdot}7H_2O$ and H_2O_2). When the $SAC_{CA\text{-}PF}$ adsorbed the CR after 720 min, the SAC was treated by Fenton's reagent before reusing it. The results of $SAC_{CA\text{-}PF}$ regeneration for five times (for a different time) are shown in Fig. 12.

The multiple utilization of adsorbents was a basic criterion for assessing their potential for practical application. The mechanism of the Fenton reaction included the reaction of ferrous ions and hydrogen peroxide to generate hydroxyl radicals (•OH). Fenton oxidation was dependent on the generation of •OH, which can react quickly with the organic pollutants [28]. The performance of the composite was verified after five recovery cycles using the Fenton oxidation process (Fig. 12). The results showed that the adsorption effect of $SAC_{CA\text{-}PF}$ on CR decreased after the first regeneration. Although the removal efficiency after five cycles is lower than that of the first cycle, the reduction rate is acceptable, exceeding 80%. Two main reasons can explain the decline in the SAC performance. First of all, the incomplete removal of dye molecules during the adsorption process led to the unavailability of some adsorption sites for the materials. Secondly, hydrogen peroxide may react with inorganic materials, which destroys the functional properties of SAC up to a certain extent [49]. In general, the experimental results showed that the adsorption efficiency of $SAC_{CA\text{-}PF}$ on CR recovery was satisfactory.

3.8. Practical application tests of the SAC

The developed SAC adsorbent was mainly used for environmental protection, such as wastewater treatment in the dye industry, etc. Different concentrations and different types of dyes were tested with $SAC_{CA\text{-}PF}$. In addition, adsorbent products were designed and tested in the laboratory.

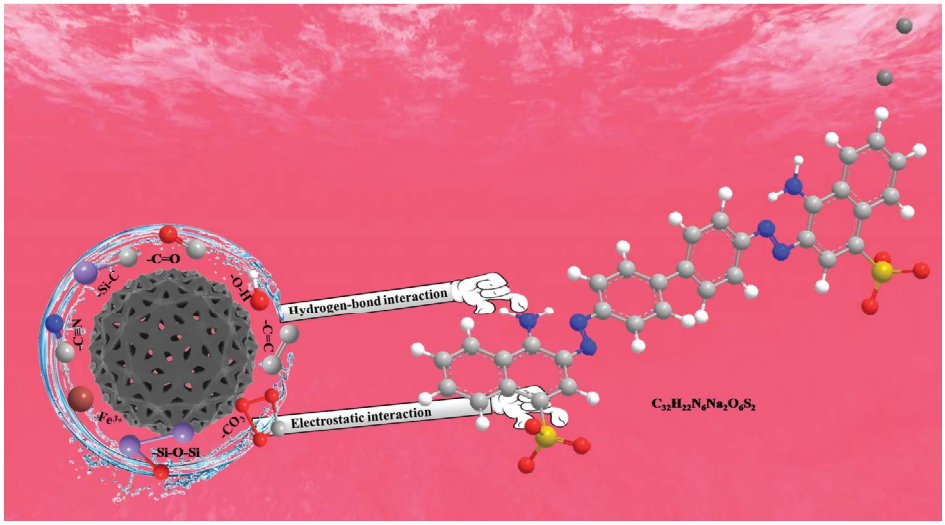

Fig. 10. Possible mechanism of CR dye adsorption on $SAC_{CA\text{-}PF}$.

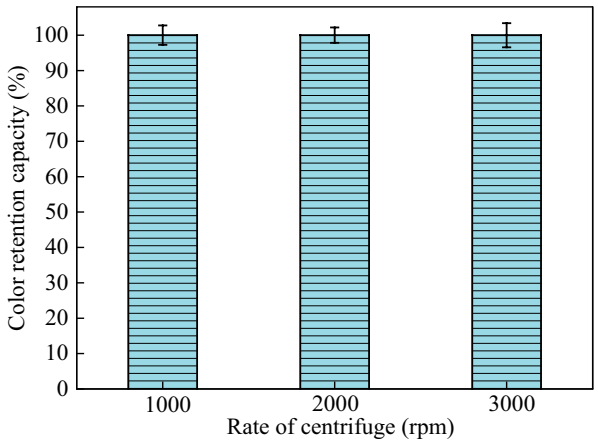

Fig. 11. The color retention capacity of the SAC_{CA-PF} at different centrifuge rate (*T*: 25°C; pH: 6; dose of SAC: 0.2 g; volume of solution: 20 mL).

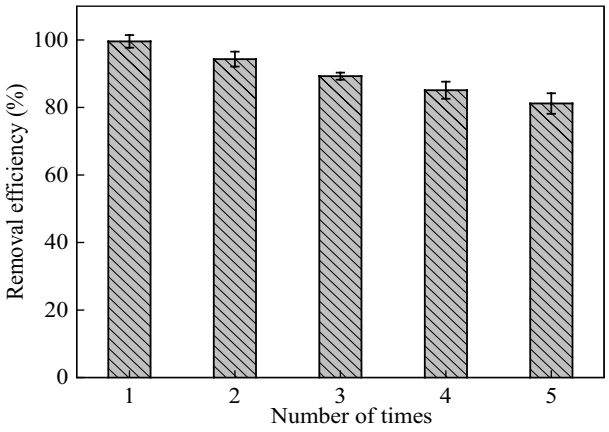

Fig. 12. The regeneration cycle of CR adsorption by SAC_{CA-PF} adsorbent was tested by Fenton method (CR: 200 mg L^{-1}; *T*: 25°C; pH: 6; dose of SAC: 0.2 g; time: 720 min).

3.8.1. Adsorption efficiency of SAC for different concentrations of dye

As shown in Fig. 13, the amount of adsorption increased with an increase in the concentration (when the same amount of SAC_{CA-PF} was added). When the initial concentration was increased from 100 to 200 mg L^{-1}, the adsorption amount increased significantly. When the concentration exceeded 300 mg L^{-1}, the adsorption amount increased very slowly. This may be because, at a high concentration, the adsorption performance by SAC_{CA-PF} got saturated along with a reduction in the adsorption sites. However, it was seen that SAC_{CA-PF} could also be well applied in the treatment of highly concentrated wastewater, such as wastewater containing industrial dye, and showed a great prospect for certain applications in the future.

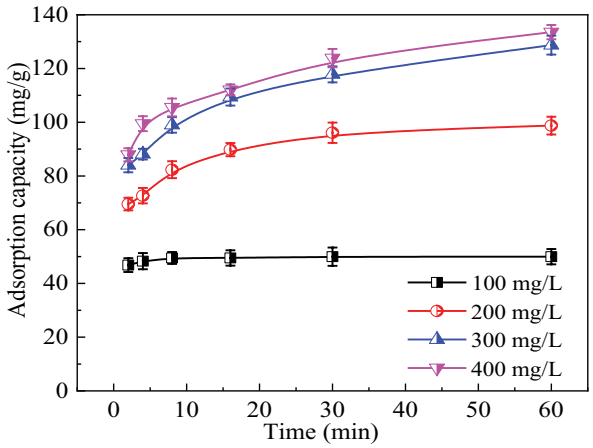

Fig. 13. The effect of different initial concentration on CR adsorption of SAC_{CA-PF} (*T*: 25°C; pH: 6; dose of SAC: 0.2 g).

3.8.2. Adsorption applications of SAC for three different dyes

By comparing the three different dyes in Fig. 14, it is found that SAC_{CA-PF} had a better adsorption effect on CR and RB, and the adsorption efficiency was almost equal in both cases. In comparison, the adsorption efficacy of SAC with respect to MB was obviously poor, and the adsorption amount does not change much with time. This may be because the surface of the adsorbent was positively charged, so the adsorption of anionic and neutral dyes was better, but the positive charge of the cationic dyes and the surface of the adsorbent exerted repulsion to each other [30]. At the same time, it was observed that under a certain concentration and dosage of adsorbent, the rate of adsorption gradually becomes flat with further adsorption, which indicated the saturation of active sites on the surface of the adsorbent [50].

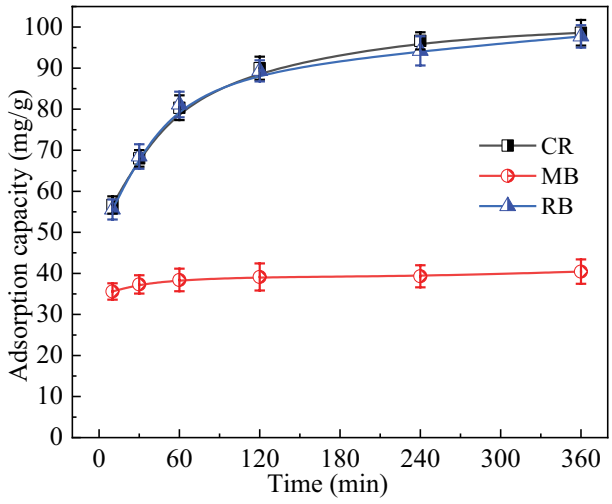

Fig. 14. SAC_{CA-PF} adsorption of different dyes (CR: 200 mg L^{-1}; *T*: 25°C; dose of SAC: 0.2 g).

4. Conclusions

The SAC_{CA-PF} was successfully prepared by the 'double green activation' method with the mixture of $C_6H_8O_7$ and K_2FeO_4 activators. Compared with the other three kinds

of SAC, the $SAC_{CA\text{-}PF}$ had the highest specific surface area (136 m^2 g^{-1}) and abundant functional groups attached to the surface. The adsorption capacity of $SAC_{CA\text{-}PF}$ for CR was the highest (98.61 mg g^{-1}) in the SAC, the adsorption was mainly affected by the chemical adsorption and monolayer adsorption process. The adsorption mechanism of CR by $SAC_{CA\text{-}PF}$ involved hydrogen bonding, electrostatic attraction, and ion interaction. The study could provide technical support for carbonized sludge and dye wastewater treatment in an environment-friendly way.

Acknowledgements

This research was supported by the National Key R&D Program of China (2020YFC1908601, 2020YFC1908602). Science Development Fund Project of Hefei University (22040521004).

References

[1] H. Gu, W. Lin, S. Sun, C. Wu, F. Yang, Z. Ye, N. Chen, J. Ren, S. Zheng, Calcium oxide modification of activated sludge as a low-cost adsorbent: preparation and application in Cd(II) removal, Ecotoxicol. Environ. Saf., 209 (2021) 111760, doi: 10.1016/j.ecoenv.2020.111760.

[2] R. Guan, X. Yuan, Z. Wu, L. Jiang, Y. Li, G. Zeng, Principle and application of hydrogen peroxide based advanced oxidation processes in activated sludge treatment: a review, Chem. Eng. J., 339 (2018) 519–530.

[3] Y. Liu, X. Kang, X. Li, Z. Wang, Z. Jin, Performance and mechanism of sludge dewaterability enhanced by potassium ferrate pretreatment and calcium chloride addition, J. Water Reuse Desal., 7 (2017) 136–141.

[4] T. Kopac, Hydrogen storage characteristics of bio-based porous carbons of different origin: a comparative review, Int. J. Energy Res., 45 (2021) 20497–20523.

[5] P. Hadi, X. Meng, N. Chao, C. Lin, G. Mckay, A critical review on preparation, characterization and utilization of sludge-derived activated carbons for wastewater treatment, Chem. Eng. J., 260 (2015) 895–906.

[6] R. Chitongo, B.O. Opeolu, O.S. Olatunji, Abatement of amoxicillin, ampicillin, and chloramphenicol from aqueous solutions using activated carbon prepared from grape slurry, Clean Soil Air Water, 47 (2019) 1800077, doi: 10.1002/clen.201800077.

[7] L. Wang, Y. Chang, Q. Liu, Fate and distribution of nutrients and heavy metals during hydrothermal carbonization of sewage sludge with implication to land application, J. Cleaner Prod., 225 (2019) 972–983.

[8] A. Raheem, V. Sikarwar, J. He, W. Dastyar, Opportunities and challenges in sustainable treatment and resource reuse of sewage sludge: a review, Chem. Eng. J., 337 (2018) 616–641.

[9] C. Liu, Z. Tang, Y. Chen, S. Su, Characterization of mesoporous activated carbons prepared by pyrolysis of sewage sludge with pyrolusite, Bioresour. Technol., 101 (2010) 1097–1101.

[10] P. Devi, A.K. Saroha, Utilization of sludge based adsorbents for the removal of various pollutants: a review, Sci. Total Environ., 578 (2017) 16–33.

[11] J. Yener, T. Kopac, G. Dogu, T. Dogu, Dynamic analysis of sorption of methylene blue dye on granular and powdered activated carbon, Chem. Eng. J., 144 (2008) 400–406.

[12] A.M. Ghaedi, M. Ghaedi, P. Karami, Comparison of ultrasonic with stirrer performance for removal of sunset yellow (SY) by activated carbon prepared from wood of orange tree: artificial neural network modeling, Spectrochim. Acta, Part A, 138 (2015) 789–799.

[13] J. Yener, T. Kopac, G. Dogu, T. Dogu, Adsorption of Basic Yellow 28 from aqueous solutions with clinoptilolite and amberlite, J. Colloid Interface Sci., 294 (2006) 255–264.

[14] J. Yener, T. Kopac, G. Dogu, T. Dogu, Batch adsorber rate analysis of methylene blue on amberlite and clinoptilolite, Sep. Sci. Technol., 41 (2006) 1857–1879.

[15] N. Dehghanian, M. Ghaedi, A. Ansari, A. Ghaedi, A. Vafaei, M. Asif, A random forest approach for predicting the removal of Congo red from aqueous solutions by adsorption onto tin sulfide nanoparticles loaded on activated carbon, Desal. Water Treat., 57 (2016) 9272–9285.

[16] E.B. Mostafa, M. Ahmed, B. Gao, X. Yin, A. Zahoor, H. Wang, Sorption of lead ions onto oxidized bagasse-biochar mitigates Pb-induced oxidative stress on hydroponically grown chicory: experimental observations and mechanisms, Chemosphere, 208 (2018) 887–898.

[17] J. Ma, B. Zhou, H. Zhang, W. Zhang, Fe/S modified sludge-based biochar for tetracycline removal from water, Powder Technol., 364 (2019) 889–900.

[18] J. Liu, Z. Huang, Z. Chen, Resource utilization of swine sludge to prepare modified biochar adsorbent for the efficient removal of Pb(II) from water, J. Cleaner Prod., 257 (2020) 120322, doi: 10.1016/j.jclepro.2020.120322.

[19] G. Jaria, V. Calisto, C.P. Silva, M.V. Gil, M. Otero, V.I. Esteves, Obtaining granular activated carbon from paper mill sludge – a challenge for application in the removal of pharmaceuticals from wastewater, Sci. Total Environ., 653 (2019) 393–400.

[20] D. Liu, Y. Tao, K. Li, J. Yu, Influence of the presence of three typical surfactants on the adsorption of nickel(II) to aerobic activated sludge, Bioresour. Technol., 126 (2012) 56–63.

[21] K.M. Smith, G.D. Fowler, S. Pullket, N.J.D. Graham, Sewage sludge-based adsorbents: a review of their production, properties and use in water treatment applications, Water Res., 43 (2019) 2569–2594.

[22] T. Kopac, E. Sulu, A. Toprak, Effect of KOH treatment on bituminous coal for the effective removal of Basic Blue 41 dye from aqueous solutions, Desal. Water Treat., 57 (2016) 29007–29018.

[23] O. Ioannidou, A. Zabaniotou, Agricultural residues as precursors for activated carbon production – a review, Renewable Sustainable Energy Rev., 11 (2007) 1966–2005.

[24] X. Yang, G. Xu, H. Yu, Z. Zhang, Preparation of ferric-activated sludge-based adsorbent from biological sludge for tetracycline removal, Bioresour. Technol., 211 (2016) 566–573.

[25] Q. Yang, X. Wang, W. Luo, J. Sun, Effectiveness and mechanisms of phosphate adsorption on iron-modified biochars derived from waste activated sludge, Bioresour. Technol., 247 (2018) 537–544.

[26] M. Inyang, E. Dickenson, The potential role of biochar in the removal of organic and microbial contaminants from potable and reuse water: a review, Chemosphere, 134 (2015) 232–240.

[27] O. Duman, C.Ö. Diker, S. Tunç, Development of highly hydrophobic and superoleophilic fluoro organothiol-coated carbonized melamine sponge/rGO composite absorbent material for the efficient and selective absorption of oily substances from aqueous environments, J. Environ. Chem. Eng., 9 (2021) 105093, doi: 10.1016/j.jece.2021.105093.

[28] Y. Wu, X.-T. Yang, F. Xin, X.-R. Cheng, Hydrothermal conversion of waste cartons into a magnetic carbon-iron composite for use as an efficient and recyclable dye adsorbent, J. Colloid Interface Sci., 578 (2020) 717–725.

[29] A.F.M. Streit, L.N. Côrtes, S.P. Druzian, M. Godinho, G.C. Collazzo, D. Perondi, G.L. Dotto, Development of high quality activated carbon from biological sludge and its application for dyes removal from aqueous solutions, Sci. Total Environ., 660 (2019) 277–287.

[30] L. Hu, C. Guang, Y. Liu, Z. Su, Adsorption behaviour of dyes from an aqueous solution onto composite magnetic lignin adsorbent, Chemosphere, 246 (2020) 125757, doi: 10.1016/j.chemosphere.2019.125757.

[31] B. Li, F. Dai, Q. Xiao, L. Yang, J. Shen, C. Zhang, M. Cai, Nitrogen-doped activated carbon for a high energy hybrid supercapacitor, Energy Environ. Sci., 9 (2016) 102–106.

[32] L. Yang, Y. Zhan, Y. Gong, E. Ren, Development of eco-friendly CO_2-responsive cellulose nanofibril aerogels as "green"

adsorbents for anionic dyes removal, J. Hazard. Mater., 405 (2021) 124194, doi: 10.1016/j.jhazmat.2020.124194.
[33] A.H. Jawad, N.S.A. Mubarak, A.S. Abdulhameed, Tunable Schiff's base-cross-linked chitosan composite for the removal of reactive red 120 dye: adsorption and mechanism study, Int. J. Biol. Macromol., 142 (2020) 732–741.
[34] A.F.M. Streit, G.C. Collazzo, S.P. Druzian, R.S. Verdi, E.L. Foletto, L.F.S. Oliveira, G.L. Dotto, Adsorption of ibuprofen, ketoprofen, and paracetamol onto activated carbon prepared from effluent treatment plant sludge of the beverage industry, Chemosphere, 262 (2021) 128322, doi: 10.1016/j.chemosphere.2020.128322.
[35] O. Duman, E. Ayranci, Structural and ionization effects on the adsorption behaviors of some anilinic compounds from aqueous solution onto high-area carbon-cloth, J. Hazard. Mater., 120 (2005) 173–181.
[36] C. Patra, R. Gupta, D. Bedadeep, S. Narayanasamy, Surface treated acid-activated carbon for adsorption of anionic azo dyes from single and binary adsorptive systems: a detail insight, Environ. Pollut., 266 (2020) 115102, doi: 10.1016/j.envpol.2020.115102.
[37] O. Pezoti, A.L. Cazetta, K.C. Bedin, L.S. Souza, A.C. Martins, T.L. Silva, O.O. Santos, J.V. Visentainer, V.C. Almeida, NaOH-activated carbon of high surface area produced from guava seeds as a high-efficiency adsorbent for amoxicillin removal: kinetic, isotherm and thermodynamic studies, Chem. Eng. J., 288 (2016) 778–788.
[38] X. Kang, Y. Liu, C. Yang, H. Cheng, Removal of amoxicillin from aqueous solution using sludge-based activated carbon modified by walnut shell and nano-titanium dioxide, J. Water Reuse Desal., 11 (2021) 97–109.
[39] S. Chowdhury, J. Sikder, T. Mandal, G. Halder, Comprehensive analysis on sorptive uptake of enrofloxacin by activated carbon derived from industrial paper sludge, Sci. Total Environ., 665 (2019) 438–452.
[40] J.P. Simonin, On the comparison of pseudo-first-order and pseudo-second-order rate laws in the modeling of adsorption kinetics, Chem. Eng. J., 300 (2016) 254–263.
[41] O. Duman, S. Tunç, B.K. Bozoğlan, T.G. Polat, Removal of triphenylmethane and reactive azo dyes from aqueous solution by magnetic carbon nanotube-κ-carrageenan-Fe_3O_4 nanocomposite, J. Alloys Compd., 687 (2016) 370–383.
[42] E. Ayranci, O. Duman, In-situ UV-visible spectroscopic study on the adsorption of some dyes onto activated carbon cloth, Sep. Sci. Technol., 44 (2009) 3735–3752.
[43] X. Guo, B. Du, W. Qin, J. Yang, Synthesis of amino functionalized magnetic graphenes composite material and its application to remove Cr(VI), Pb(II), Hg(II), Cd(II) and Ni(II) from contaminated water, J. Hazard. Mater., 278 (2014) 211–220.
[44] S. Banerjee, S. Mukherjee, A. Laminka-ot, S.R. Joshi, T. Mandal, G. Halder, Biosorptive uptake of Fe^{2+}, Cu^{2+} and As^{5+} by activated biochar derived from *Colocasia esculenta*: isotherm, kinetics, thermodynamics and cost estimation, J. Adv. Res., 7 (2016) 597–610.
[45] O. Duman, S. Tunç, T.G. Polat, Determination of adsorptive properties of expanded vermiculite for the removal of C.I. Basic Red 9 from aqueous solution: kinetic, isotherm and thermodynamic studies, Appl. Clay Sci., 109 (2015) 22–32.
[46] O. Duman, T.G. Polat, C.Ö. Diker, S. Tunç, Agar/κ-carrageenan composite hydrogel adsorbent for the removal of methylene blue from water, Int. J. Biol. Macromol., 160 (2020) 823–835.
[47] M. Ghaedi, A. Ansari, P.A. Nejad, A. Ghaedi, A. Vafaei, M.H. Habibi, Artificial neural network and bees algorithm for removal of Eosin B using cobalt oxide nanoparticle-activated carbon: isotherm and Kinetics study, Environ. Prog. Sustainable Energy, 34 (2015) 155–168.
[48] M.M. Hassan, C.M. Carr, A critical review on recent advancements of the removal of reactive dyes from dye house effluent by ion-exchange adsorbents, Chemosphere, 209 (2018) 201–219.
[49] M.A. Fard, B. Barkdoll, Using recyclable magnetic carbon nanotube to remove micropollutants from aqueous solutions, J. Mol. Liq., 249 (2018) 193–202.
[50] K.L. Yu, L.X. Jiat, H.C. Ong, W.H. Chen, Adsorptive removal of cationic methylene blue and anionic Congo red dyes using wet-torrefied microalgal biochar: equilibrium, kinetic and mechanism modeling, Environ. Pollut., 272 (2021) 115986, doi: 10.1016/j.envpol.2020.115986.